

# Design, Identification, and Control of a Flexure-Based XY Stage for Fast Nanoscale Positioning

Yuen Kuan Yong, Sumeet S. Aphale, and S. O. Reza Moheimani, *Senior Member, IEEE*

**Abstract**—The design, identification, and control of a novel, flexure-based, piezoelectric stack-actuated XY nanopositioning stage are presented in this paper. The main goal of the design is to combine the ability to scan over a relatively large range ( $25 \times 25 \mu\text{m}$ ) with high scanning speed. Consequently, the stage is designed to have its first dominant mode at 2.7 kHz. Cross-coupling between the two axes is kept to  $-35$  dB, low enough to utilize single-input–single-output control strategies for tracking. Finite-element analysis (FEA) is used during the design process to analyze the mechanical resonance frequencies, travel range, and cross-coupling between the X- and Y-axes of the stage. Nonlinearities such as hysteresis are present in such stages. These effects, which exist due to the use of piezoelectric stacks for actuation, are minimized using charge actuation. The integral resonant control method is applied in conjunction with feedforward inversion technique to achieve high-speed and accurate scanning performances, up to 400 Hz.

**Index Terms**—Feedforward inversion, integral resonant control (IRC), mechanical design, nanopositioning stage.

## I. INTRODUCTION

**F**LEXURE-BASED, piezoelectric stack-actuated nanopositioning stages have emerged as an important technological advancement in hi-tech applications, including scanning probe microscopy, lithography, nanometrology, beam steering for optical communication systems, fabrication, and assembly of nanostructures [1]–[9]. These nanopositioning stages typically have high positioning accuracy and high traveling speeds of several hundred hertz. Although piezoelectric tube scanners are widely used in scanning probe microscopy applications [10], [11], they are slowly overtaken by piezoelectric stack-actuated stages, due to their larger range of motion, greater mechanical bandwidth, and lower cross-coupling between the axes. Despite this, piezoelectric tube scanners are expected to remain a widely used

means of actuation in nanoscale positioning systems due to their low cost.

The demand for high-bandwidth nanopositioning stages is increasing, especially in the field of cell biology [1], [12]. Many approaches have been investigated to increase the bandwidth of nanopositioning stages, particularly by improving the mechanical design [13] and implementing various control algorithms on the systems [2], [14]. To improve the bandwidth mechanically, it is common practice to make the stage compact and rigid in order to achieve a high first resonance frequency for each axis [13]. However, the reduction in size results in a reduction in the travel range of the stage. An example of this is reported in [15], where the stage has a relatively small travel range of approximately  $10 \mu\text{m}$  along the X- and Y-axes, but a high first resonant mode of about 20 kHz for both axes. There is no mechanical amplification lever used in this particular design to magnify the displacement of piezoelectric stack actuators. In order to achieve a high resonance frequency with  $10\text{-}\mu\text{m}$  travel range, multiple piezoelectric stack actuators are arranged in series and in direct-drive mode to displace the stage. Most of the commercially available stages have a large travel range (up to  $100 \mu\text{m}$ ), but a low first resonance frequency (typically less than 400 Hz) and vice versa [16]. In this paper, we report the design of a stage that has a relatively large travel range ( $25 \mu\text{m}$ ) and a high resonance frequency (2.7 kHz). Cross-coupling between the two axes is the major source of error in scanning applications. Subsequently, our stage is designed to have a low cross-coupling ( $-35$  dB).

The tracking performance of these nanopositioning stages is severely limited by the hysteresis in the piezoelectric stack actuators as well as the lightly damped resonant mechanical modes. Charge actuation has been documented to provide a significant reduction in hysteresis errors [17]. A custom-built charge source capable of driving large capacitive loads such as piezoelectric stack actuators is employed in this paper. Accurate tracking is achievable using inversion-based feedforward control [18]. The lightly damped first mechanical resonant mode of the stage makes accurate inversion quite difficult. To improve tracking using the inversion-based feedforward technique, this resonant mode needs to be damped using a suitable feedback controller [19].

Passive damping techniques such as shunts have been effective but may need constant tuning. The shunt damping shows a drastic performance degradation if the resonance changes; therefore, more evolved adaptive shunts are needed to handle system uncertainties [20], [21]. Various feedback controllers

Manuscript received January 25, 2008; accepted September 3, 2008. First published September 23, 2008; current version published January 16, 2009. This work was supported in part by the Australian Research Council's Center of Excellence for Complex Dynamic Systems and Control and in part by the University of Newcastle under Early Career Researcher (ECR) Grant. The review of this paper was arranged by Associate Editor M.-F. Yu.

Y. K. Yong is with the Australian Research Council (ARC) Center for Complex Dynamic Systems and Control (CDSC), University of Newcastle, Callaghan, N.S.W. 2308, Australia (e-mail: yuenkuan.yong@newcastle.edu.au).

S. O. R. Moheimani is with the School of Electrical Engineering and Computer Science, University of Newcastle, Callaghan, N.S.W. 2308, Australia (e-mail: reza.moheimani@newcastle.edu.au).

S. S. Aphale is with the Center for Applied Dynamics Research (CADR), School of Engineering, Kings College, University of Aberdeen, U.K. (e-mail: s.aphale@abdn.ac.uk).

Color versions of one or more of the figures in this paper are available online at <http://ieeexplore.ieee.org>.

Digital Object Identifier 10.1109/TNANO.2008.2005829

that impart substantial damping to the system have been formulated and documented over the years [22]–[24]. Resonant control [25] and PPF control [26] are known to provide substantial damping to highly resonant systems. A straightforward control design approach is that of a polynomial-based controller [27]. This controller imparts substantial damping to the system, is easy to construct for second-order systems, and is robust under resonance frequency variations [28], [29]. Combining such damping controllers that are insensitive to variations in resonance frequencies with an integral controller has been reported earlier [30]. Integral resonant control (IRC) has been proposed recently to damp collocated systems [31]. It is a simple yet well-performing technique that adds substantial damping to resonant modes of the system without exciting the high-frequency dynamics. Here, this technique will be integrated with the feedforward inversion technique to deliver accurate high-speed scanning performances.

### A. Objectives and Outlines

The main objectives of this paper are:

- 1) to design a nanopositioning stage that has relatively high resonance frequency, scan range, and decoupling between its two axes;
- 2) to implement a well-performing control scheme that provides accurate high-speed scanning performance.

This paper is organized as follows. In Section II, we describe the design of a nanopositioning stage. This is followed by a discussion on a number of design considerations such as flexure parameters, material used, structural stiffness, and piezoelectric stack actuator stiffness. The FEA analysis is performed using ANSYS. The experimental setup and system identification of the stage are presented in Section III. Open-loop frequency responses as well as triangular scans are presented to verify that the stage behaves as predicted. Section IV gives the details of the IRC design as well as the inversion-based feedforward technique. Scanning results comparing the open- and closed-loop tracking performances are also presented in this section.

## II. DESIGN OF THE XY NANOPositionING STAGE

In this paper, the design of the flexure-based nanopositioning stage is based on the concept of flexible mechanisms (flexures) where motions are generated through the elastic deformation of the structures [32], [33]. There are no moving and sliding joints; therefore, the problems of wear, backlash, friction, and the need for lubrication are eliminated. This provides repeatable and smooth motions to fulfill the requirement of accurate nanoscale positioning. Two types of flexures are used in the design, circular, and beam flexures (see Fig. 1). Piezoelectric stack actuators are commonly used to drive flexure-based stages due to their capability of achieving repeatable nanometer resolution over a very high bandwidth. They can also generate large forces and high accelerations [1], which are desirable for the design of a high-bandwidth stage.

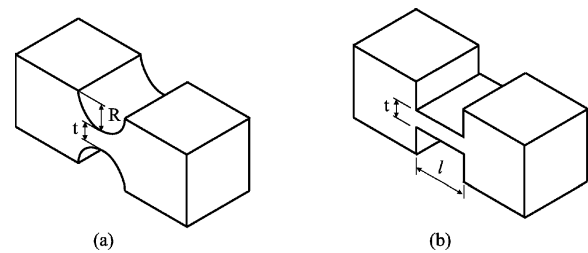


Fig. 1. Flexures. (a) Circular flexure.  $t$  is the minimum thickness and  $R$  is the radius of the curve. (b) Beam flexure.  $t$  is the minimum thickness and  $l$  is the length.

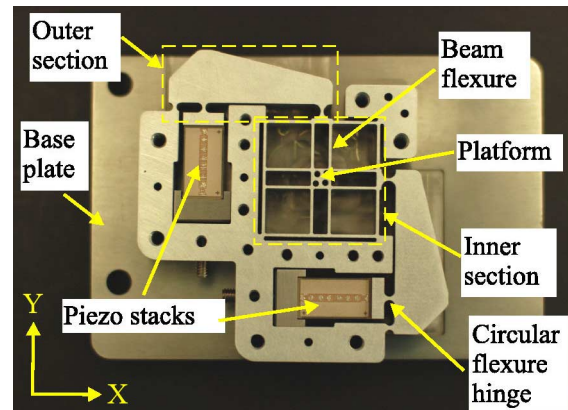


Fig. 2. Flexure-based XY nanopositioning stage. Design consists of the outer and inner sections. The outer section is designed to amplify the displacement of piezoelectric stack actuators. The inner section is designed to minimize the coupling between the X and Y motions.

### A. Design Descriptions

The nanopositioning stage consists of two main parts: 1) the outer section that consists of amplification levers and circular flexures and 2) the inner section that consists of a stage and beam flexures (see Fig. 2). There are two piezoelectric stack actuators, each providing the required input displacement to the X- and Y-axes, respectively. At the outer section, an amplification lever is integrated into each axis of the stage to amplify the displacement of the piezoelectric stack actuator. The amplified motions are transferred to the inner section to displace the platform. Fig. 3 shows the graphical representation of X and Y motions of the stage simulated using ANSYS.

Circular flexures are used in the design of the amplification levers since they provide more accurate rotational motions, i.e., the center of deflection can be estimated to be at the center of the circular flexure [34]–[36]. A minimum variation of the center of deflection is needed to obtain optimal amplification out of the lever [37], [38]. Circular flexures are also used to avoid twisting resonant modes (about the X- and Y-axes) that often occur at low frequencies. Fig. 4 shows the comparisons between the twisting resonant modes (in ANSYS) of the two amplification levers using beam and circular flexures, respectively. The beam and circular flexures have the same length ( $l = 2R$ ) and minimum thickness ( $t$ ) for comparison purposes. The simulation shows that the twisting mode corresponding to the lever with circular flexures occurs approximately 660 Hz higher

than that of the lever with beam flexures. Therefore, circular flexures are chosen for the design of the amplification lever. The amplification ratio of the lever is estimated to be approximately 2.5.

The inner section is designed to minimize the coupling between the  $X$  and  $Y$  motions of the stage. At the inner section, the stage is held by four pairs of beam flexures. The flexures are arranged in such a way so that they are rigid along the direction of motion and are flexible in the axis perpendicular to the motion [13]. Beam flexures are used to guide the stage since they are more flexible and can provide a larger motion range than circular flexures.

### B. Design Considerations

Our objective is to design a nanopositioning stage with a high first resonance frequency, a relatively high travel range, and a low cross-coupling in motion between the  $X$ - and  $Y$ -axes. To achieve a high resonance frequency, the design of the stage has to be compact and rigid [13]. As a result, the length of the flexures and the amplification levers have to be small. However, short flexures and levers will reduce the overall  $X$  and  $Y$  motions of the stage. To search for an agreeable compromise between resonance frequency and travel range, ANSYS is used to conduct a number of design iterations until the desired design criteria is achieved. The thicknesses of all the flexures are carefully taken into consideration to minimize the cross-coupling and maximize both the resonance frequency and travel range of the stage.

The resonance frequency of the stage is also dependent on the type of the material used. A material with high Young's modulus of elasticity  $E$  to density ratio  $\rho$  is preferred because a stiff and light material (high  $E$  and low  $\rho$ ) will improve the mechanical stiffness and bandwidth of the stage. Aluminum alloy 7075 (Al 7075), with  $E = 72$  GPa and  $\rho = 2.81$  g/cm<sup>3</sup> (a relatively high value of  $E/\rho$ ), is used to fabricate the stage.

The structural stiffness ( $k_s$ ) of the stage (which is experienced by the piezoelectric stack actuator) is also carefully considered in the design process. This is because the maximum displacement of the piezoelectric stack actuator is governed by  $k_s$  as follows [16]:

$$\Delta L = \frac{k_{\text{piezo}}}{k_s + k_{\text{piezo}}} \Delta L_o \quad (1)$$

where  $\Delta L_o$  is the maximum nominal displacement of a piezoelectric stack actuator without external spring load,  $\Delta L$  is the displacement with external spring load,  $k_s$  is the structural stiffness of the stage, and  $k_{\text{piezo}}$  is the piezoelectric stack actuator stiffness.

In order to increase the resonance frequencies of the stage, a high value of  $k_s$  is required. However, the increase of the stiffness will result in a decrease in the maximum displacement ( $\Delta L$ ) of the piezoelectric stack actuator. To reach an acceptable compromise between the resonance frequency and the travel range of the stage,  $k_s$  is chosen to be approximately 20% of  $k_{\text{piezo}}$ . For the best result, a piezoelectric stack actuator with large  $k_{\text{piezo}}$  is selected; thus, the stage can be designed to have a

TABLE I  
TECHNICAL DATA OF THE PIEZOELECTRIC STACK ACTUATOR USED IN THE DESIGN OF THE NANOPositionING STAGE

Dimension (mm)	Nominal displacement ( $\mu\text{m}$ @ 100V)	Stiffness (N/ $\mu\text{m}$ )	Resonance freq. (kHz $\pm 20\%$ )
10 $\times$ 10 $\times$ 18	15 $\pm 10\%$	200	70

large  $k_s$  and high mechanical resonance frequency without losing too much of its travel range. A piezoelectric stack actuator P-888.50<sup>1</sup> is selected for the design. Detailed technical specifications of the piezoelectric stack actuator are shown in Table I. The  $k_{\text{piezo}}$  of this piezoelectric stack actuator is 200 N/ $\mu\text{m}$ , which is well suited for the design requirement mentioned before. The final design of the stage is predicted to have a first resonance frequency of 2.5 kHz, a travel range of 25  $\mu\text{m}$ , and a cross-coupling of  $-35$  dB. The FEA simulation of the first resonance frequency along the  $X$ - and  $Y$ -axes of the stage can be found in Fig. 3.

### III. EXPERIMENTAL SETUP AND SYSTEM IDENTIFICATION

In this section, we describe the experimental setup and characterization of the  $XY$  nanopositioning stage. Using the design results predicted by ANSYS, the stage is fabricated using Al 7075 with a thickness of 12.8 mm. Wire-electrical-discharge-machining (WEDM) technique is used to fabricate the stage due to its accuracy and precision [39]. The stage is mounted on a 10-mm steel plate to be rigidly held in place. A small aluminum block with a fine surface finish is attached to the nanopositioning stage, as shown in Fig. 5. This block is used as the target for displacement sensing. It also serves as a stage over which a sample can be placed and moved. Two ADE Technologies 8810 capacitive sensors (which have a static gain of 2.5  $\mu\text{m}/\text{V}$ ) are placed in close proximity to the adjacent surfaces of the aluminum block to measure the displacements along the  $X$ - and  $Y$ -axes.

Fig. 5 shows the experimental setup used for this study. To clarify the associated gains of the system, a block diagram is presented in Fig. 6. A Stanford Research Systems Preamplifier was used to improve the resolution of the dSPACE analog-to-digital converter (ADC)/digital-to-analog converter (DAC) boards and minimize quantization noise. The preamplifier gain was set to 10 but was taken out of the data when plotting; thus, the dc gain of the system from digital signal analyzer (DSA) input to capacitive sensor output is unity (0 dB), as shown in Fig. 7. The piezoelectric stack actuators were driven by the charge amplifier that has a gain of 126  $\mu\text{C}/\text{V}$  and an equivalent voltage gain of 10. Hysteresis due to the use of piezoelectric stack actuators is minimized using charge actuation. The benefit of using charge actuation is demonstrated in Fig. 8. Without using the charge actuation, the hysteresis loop is approximately 3  $\mu\text{m}$  wide (12.6% of the maximum stage displacement) compared to 0.33  $\mu\text{m}$  (1.6%) when the charge actuation is used.

To identify the linear model within the bandwidth of interest, the plant was identified using a band-limited random noise input of amplitude 300 mV<sub>pk</sub> within the frequency range of

<sup>1</sup>A product of Physik Instrumente.

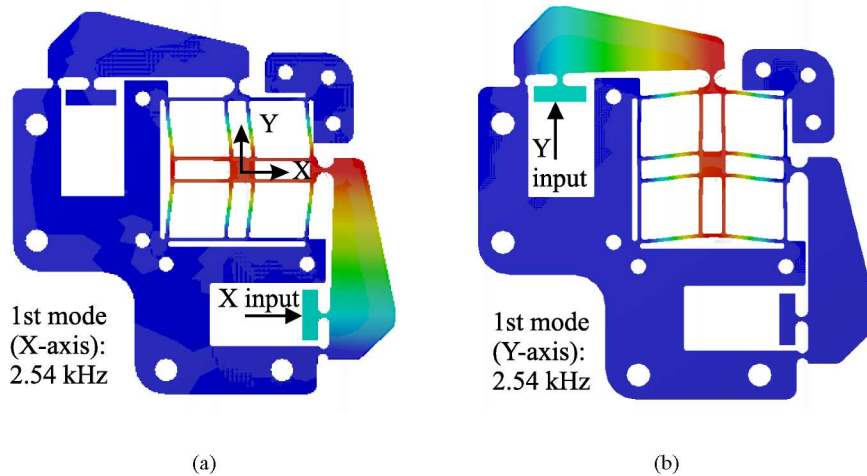


Fig. 3. ANSYS simulation of motions and resonance frequencies of the nanopositioning stage. (a) Simulation results for the  $X$ -axis. (b) Simulation results for the  $Y$ -axis.

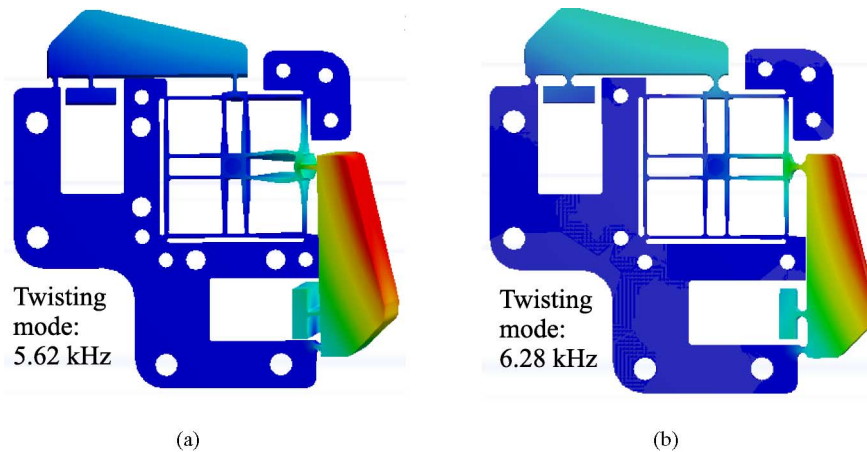


Fig. 4. Twisting resonant modes of amplification levers. (a) With beam flexures, the resonant mode is found at 5.62 kHz. (b) With circular flexures, the resonant mode is found at 6.28 kHz.

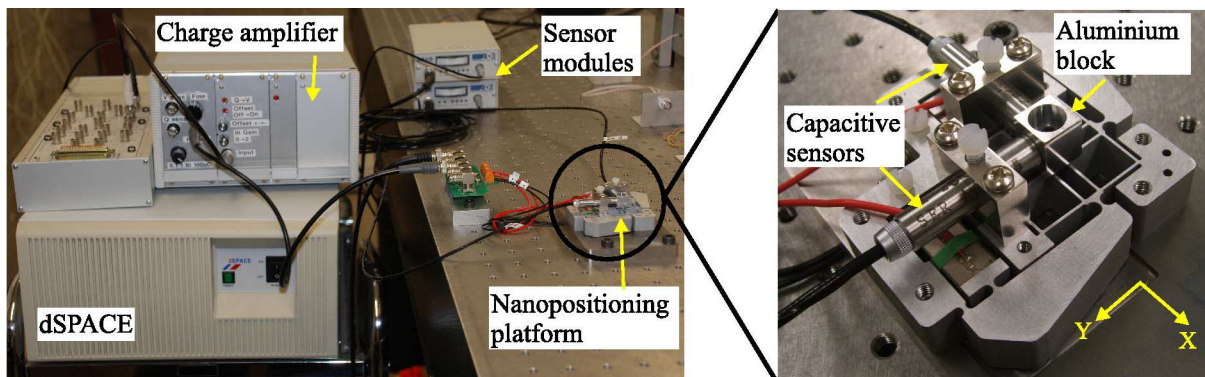


Fig. 5. Experimental setup of the  $XY$  nanopositioning stage. A dSPACE rapid prototyping system with 16-bit ADC (DS2001)/DAC (DS2102) cards is used to implement control strategies. The nanopositioning stage is driven using a charge amplifier that has a gain of  $126 \mu\text{C}/\text{V}$ . Capacitive sensors are incorporated to measure the  $X$  and  $Y$  motions of the stage. The aluminium block is machined to have a fine surface finish and is used as the sensing target.

10 Hz–10 kHz, using an HP 35670A dual-channel spectrum analyzer. The stage is a two-input–two-output system. Input signals applied to the piezoelectric stacks in the  $X$ - and  $Y$ -directions are denoted as  $u_x$  and  $u_y$  (in volts), respectively, and the outputs are

the respective stage displacements  $d_x$  and  $d_y$  (in micrometers) given by the capacitive sensors as corresponding voltages. Random noise input signals ( $u_x$  and  $u_y$ ) generated by the spectrum analyzer are applied to the  $X$ - and  $Y$ -axes piezoelectric stack

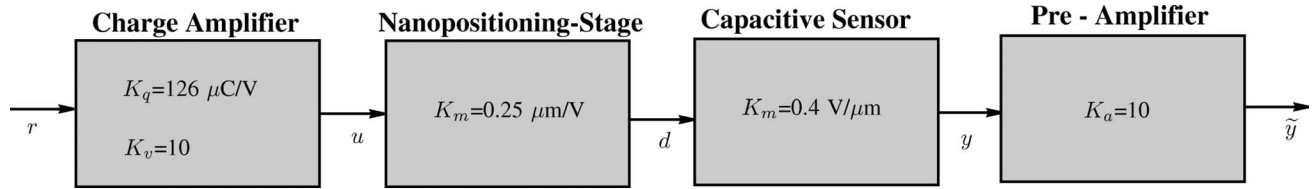


Fig. 6. Gains associated with the experimental setup.  $r$  is the reference input in volts, generated by the DSA,  $u$  is the output of the charge amplifier in microcoulombs used as the driving input for the nanopositioning stage,  $d$  is the actual displacement of the nanopositioning stage in micrometers, and  $y$  is the proportionally scaled capacitive sensor output in volts. To improve the resolution and minimize quantization noise of the dSPACE ADC/DAC channels, a gain of 10 was introduced during measurement using a preamplifier. This gain was taken out while plotting the frequency responses given in Fig. 7. Thus, the frequency responses are from input  $r$  to output  $y$ .

actuators respectively through the charge amplifier. The capacitive sensor outputs ( $d_x$  and  $d_y$ ) are, respectively, measured and fed back to the spectrum analyzer to construct the corresponding frequency responses. The transfer functions of the frequency response can be described as  $G_{xx}(j\omega) = d_x(j\omega)/u_x(j\omega)$ ,  $G_{yx} = d_y(j\omega)/u_x(j\omega)$ ,  $G_{xy}(j\omega) = d_x(j\omega)/u_y(j\omega)$ , and  $G_{yy}(j\omega) = d_y(j\omega)/u_y(j\omega)$ . Here,  $u_x(j\omega)$ ,  $u_y(j\omega)$ ,  $d_x(j\omega)$ , and  $d_y(j\omega)$  denote the Fourier transforms of  $u_x$ ,  $u_y$ ,  $d_x$ , and  $d_y$ , respectively. Fig. 7 plots the frequency responses of the stage.

In Fig. 7, the first resonant peak of the stage (at both axes) is observed at 2.7 kHz, about 8% higher than the predicted value of ANSYS simulations. The magnitude of the cross-coupling terms  $G_{yx}$  and  $G_{xy}$  are about  $-35$  dB and  $-40$  dB less than that of  $G_{xx}$  and  $G_{yy}$ , respectively. The measured  $G_{yx}$  is in close agreement with that obtained from ANSYS simulations. However, there are some differences between the  $G_{xy}$  values. These are most likely due to the fact that piezoelectric stack actuators are not properly modeled. The differences could also be partially due to manufacturing tolerances and machining imperfections [40].

The scanning range of the stage is measured by applying a low-frequency triangular signal with a peak-to-peak voltage equal to the maximum voltage that could be applied to this specific piezoelectric stack actuator, i.e., 100 V. As the piezoelectric stack was driven using charge, it was ascertained that the maximum voltage across the piezoelectric stack did not go beyond 100 V. The displacement was measured and is plotted in Fig. 9. The measured travel range is  $25 \mu\text{m}$ , which is in close agreement to the predicted value from ANSYS analysis.

Open-loop traces of a triangular waveform are obtained at 10, 20, 30, and 40 Hz (see Fig. 10). Earlier stage designs produced acceptable scans at very low frequencies ( $f \leq 1$  Hz) [16]. It can be seen clearly that the stage produces open-loop scans accurately at frequencies of 10 and 20 Hz. The 30-Hz triangular input excites the first resonance of the stage. This effect is more prominent in the 40-Hz scan. To increase the positioning bandwidth of the stage, both damping and tracking control strategies need to be implemented. In the next section, the details of the IRC scheme for damping and the inversion-based feedforward scheme for tracking are presented.

#### IV. CONTROL DESIGN

The dominant resonant peak of the stage occurs at 2.73 kHz and has a dynamic range of 39 dB. As the other two modes of the identified system are quite far away from the first one and have

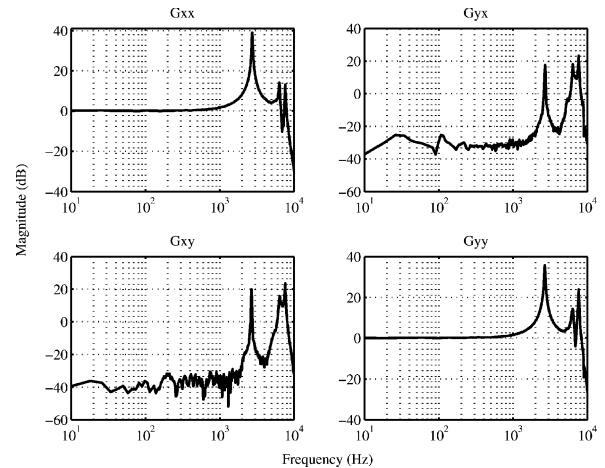


Fig. 7. Measured frequency responses of the two-input–two-output nanopositioning stage. The input is reference voltage  $r$  and the output is capacitive sensor voltage  $y$  corresponding to stage displacement  $d$  in micrometers, as shown in Fig. 6. Note that the nanopositioning stage is driven using a charge amplifier that produces a charge proportional to the reference voltage  $r$  using a gain of  $126 \mu\text{C}/\text{V}$ .

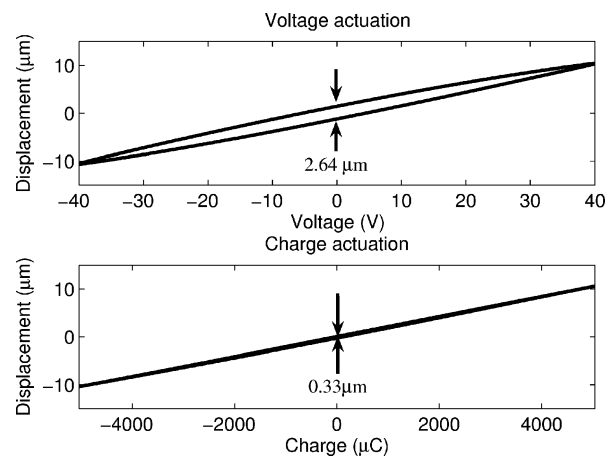


Fig. 8. Hysteresis curves for voltage and charge actuations. Input is in voltage (V) and charge ( $\mu\text{C}$ ), respectively. Output is the stage displacement in micrometers.

a much lower dynamic range, only the first mode is prioritized. The IRC scheme is an effective method of introducing substantial damping to the system. It also has a desirable property of not exciting the higher frequency dynamics. The method followed to implement a suitable IRC scheme is discussed shortly.

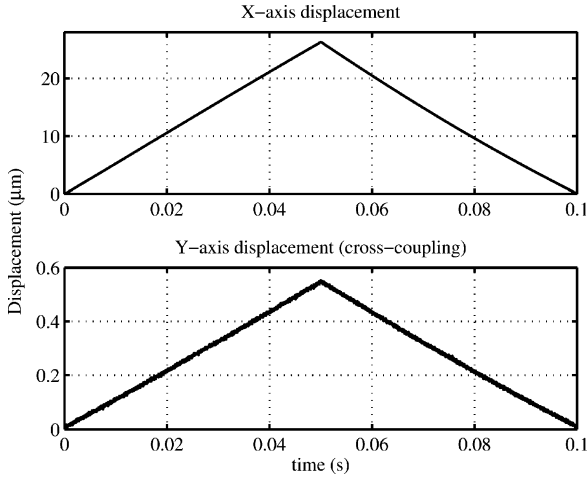


Fig. 9. Full scanning range of the nanopositioning stage is  $25 \mu\text{m}$ . The cross-coupling measured on the other axis is less than 2%. This is also validated by the frequency response data shown in Fig. 7.

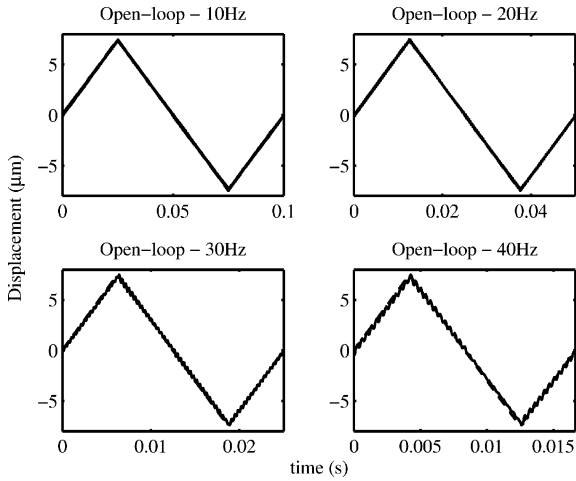


Fig. 10. Tracking performance in open loop at 10, 20, 30, and 40 Hz. Triangular reference signal (dashed line) and output signal (solid line) are plotted. The first resonant mode of the stage is excited at 30 Hz.

*Step 1:* A second-order model is fitted to the frequency response of the plant such that it accurately captures the dominant resonant mode of the stage. The transfer function of this model is given by

$$G_{\text{model}} = \frac{-0.01s^2 - 1.376s + 2.929 \times 10^8}{s^2 + 137.6s + 2.958 \times 10^8}. \quad (2)$$

The model is identified using the subspace-based modeling method from the measured open-loop frequency response function data [41].

*Step 2:* Table II gives the location of the poles and zeros for the second-order plant model  $G_{\text{model}}$  and the overall system with a feedthrough term  $G_{\text{model}} + D$ . Using a suitable feedthrough term  $D$ , the right half-plane zero can be shifted to the left half-plane, thus making the overall plant  $G_{\text{model}} + D$  conducive to integral feedback. In this case, a feedthrough term of  $D = -4$

TABLE II  
LOCATION OF POLES AND ZEROS FOR THE SECOND-ORDER PLANT MODEL  $G_{\text{model}}$  AND THE OVERALL SYSTEM WITH THE FEEDTHROUGH TERM  $G_{\text{model}} + D$

System	Poles	Zeros
$G_{\text{model}}$	$-68.8 \pm 1.72 \times 10^4 i$	$\pm 3.85 \times 10^4$
$G_{\text{model}} + D$	$-68.8 \pm 1.72 \times 10^4 i$	$-68.8 \pm 1.45 \times 10^4 i$

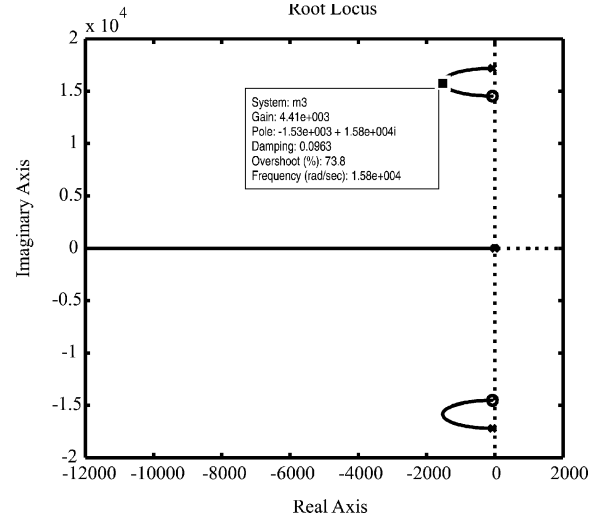


Fig. 11. Root locus plot of the loop shows the trajectory that the pole travels with respect to increase in gain to finally reach zero. Note that maximum damping is achieved when the system gain is 4410. This gain is implemented in the actual setup.

when added to the system will render it minimum phase.

*Step 3:* A unity gain negative integrator ( $-1/s$ ), was simulated in negative feedback with the overall plant and a root locus plot was obtained (see Fig. 11). A gain of 4410 achieves maximum damping.

Thus, for Fig. 12(a) and (b),  $K = -4410$  and  $D = -4$ . The overall controller has a low-pass filter type characteristics and the system can be simplified to the one shown in Fig. 12(b). Fig. 13(a) shows the simulation results obtained using the measured open-loop frequency response data.

The implemented control scheme damps the dominant resonant mode effectively by 28 dB [see Fig. 13(b)]. These results match with the simulation results shown in Fig. 13(a) quite accurately. The plant has been identified up to 10 kHz, and the control scheme does not have any adverse effect on the high-frequency dynamics. Note that the dc gain of the closed-loop system is 0.4, i.e., to get one-unit output, the closed-loop system needs an input of 2.5 units. Also note that as  $K = -4410$  (negative), the output is  $180^\circ$  out of phase with the input. The gain as well as the phase shift are automatically taken into account by the feedforward inversion technique. The control strategy was implemented using a dSPACE-1005 rapid prototyping system equipped with 16-bit ADC (DS2001)/DAC (DS2102) cards. To ensure that there are no aliasing effects, a sampling frequency of 40 kHz was chosen.

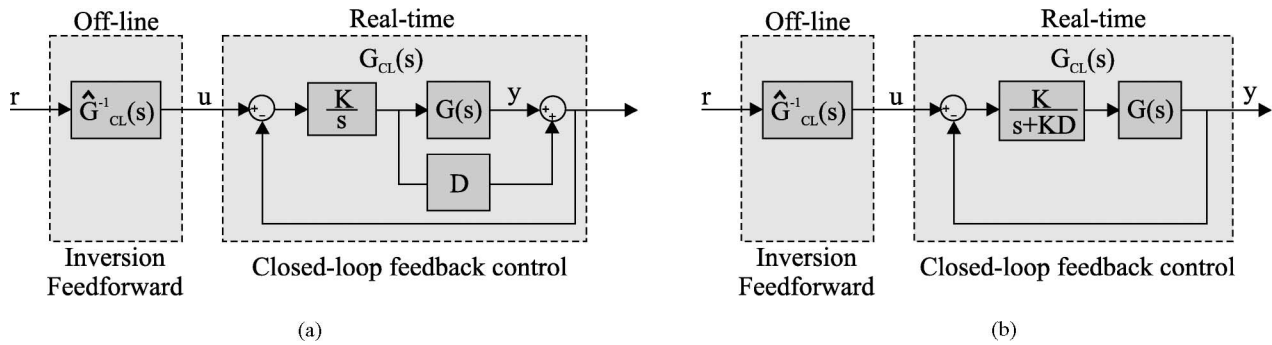


Fig. 12. Block diagrams of the IRC scheme. (a) IRC with inversion feedforward. (b) Simplified IRC that has a low-pass filter characteristic. Note that in this case, both  $K$  and  $D$  are negative.

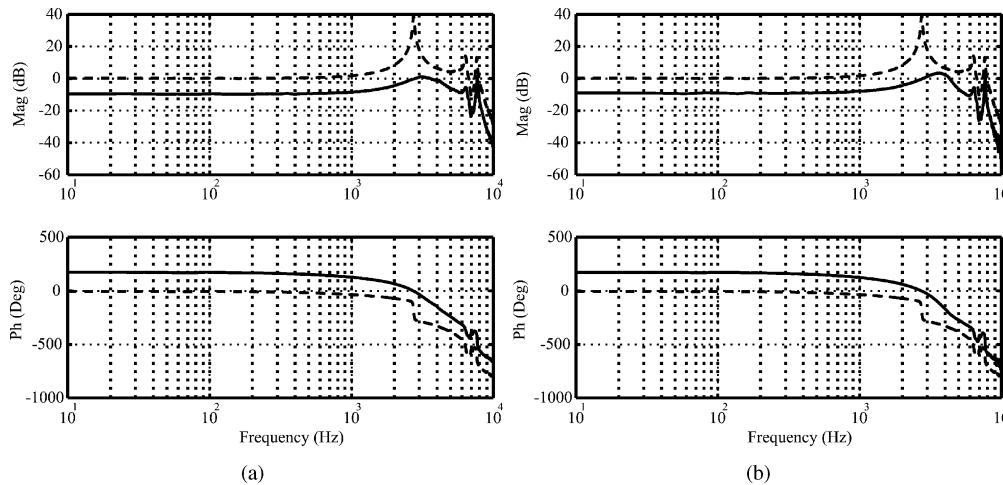


Fig. 13. Simulated (a) and measured (b) frequency response of the nanopositioning stage for open-loop (dashed line) and closed-loop damped system with IRC scheme (solid line).

## V. SCANNING RESULTS

In this section, the scanning performance of the stage is evaluated using triangular waveforms. The inversion-based feedforward approach is based on accurate model identification. After examining the closed-loop data, it was deemed feasible to invert the model in the frequency range of 0 Hz–5.4 kHz. To evaluate the high-speed scanning performance of the nanopositioning stage, triangular waveforms with fundamental frequencies of 100, 200, 300, and 400 Hz were chosen. The open-loop scans are plotted in Fig. 14. Inversion-based inputs are obtained by using all the odd harmonics of the fundamental frequency of the triangular wave that lie within the bandwidth of 0 Hz–5.4 kHz. Thus, the 100-Hz inversion-based input is obtained using the first 54 harmonics, and the 200-Hz input is obtained using the first 27 harmonics. Similarly, 18 harmonics are included in the 300-Hz input and 13 harmonics are included in the 400-Hz input. Fig. 15 plots the closed-loop scan obtained. It is clear that the tracking performance of the stage in closed loop is substantially superior to that in open loop.

Open- and closed-loop scans are plotted for charge actuation. To ascertain that the current limit of the charge amplifier is not exceeded, the scans were limited to  $15 \mu\text{m}$ . Table III documents the rms scanning error in nanometers, in open and closed loops

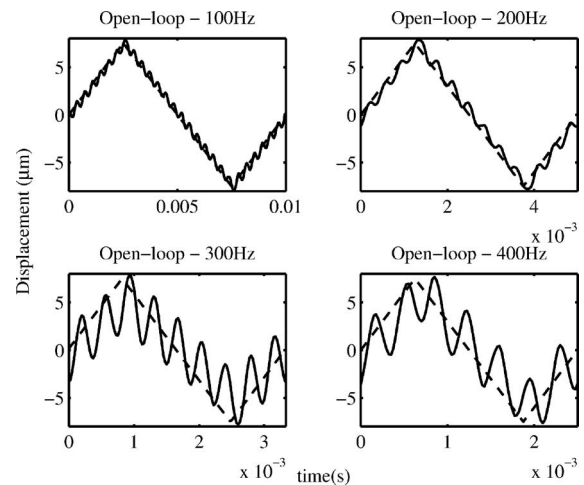


Fig. 14. Tracking performance in open loop at 100, 200, 300, and 400 Hz. Triangular reference signal (dashed line) and output signal (solid line) are plotted.

for 90% of the scanning range ( $13.5 \mu\text{m}$ ). Table IV presents the tracking error as a percentage of the scanning range. Note that in open loop, the stage never tracked within 2% of the desired trajectory. On the other hand, with the IRC and feedforward

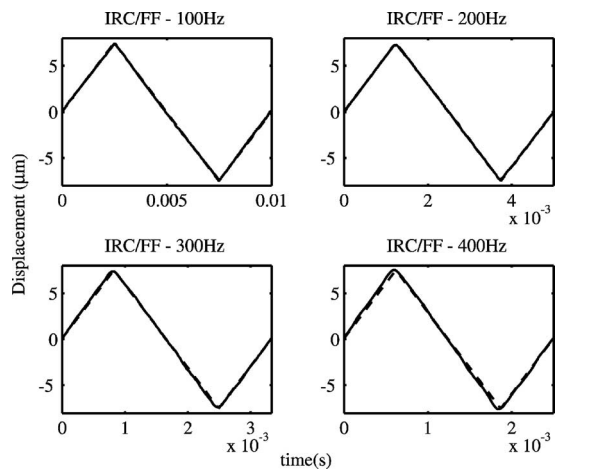


Fig. 15. Tracking performance in closed-loop at 100, 200, 300, and 400 Hz. Triangular reference signal (dashed line) and output signal (solid line) are plotted.

TABLE III

RMS ERRORS OF THE TRACKING PERFORMANCE IN OPEN AND CLOSED LOOPS FOR 90% OF THE SCANNING RANGE

RMS error (nm)	100Hz	200Hz	300Hz	400Hz
Open-loop	447	679	2254	2432
IRC+Feedforward	51	60	150	259

TABLE IV

TRACKING ERROR OBTAINED AS A PERCENTAGE OF THE SCANNING RANGE

% error	100Hz	200Hz	300Hz	400Hz
Open-loop	2.98	4.65	15.03	16.21
IRC+Feedforward	0.38	0.44	1.11	1.92

combined, the maximum percentage error is less than 2% for all the scans.

## VI. CONCLUSION

The designed nanopositioning stage has three main desirable characteristics, viz.: 1) high bandwidth; 2) relatively high motion range; and 3) low cross-coupling. These three characteristics are in close agreement with the predicted values of ANSYS analysis. With the high-bandwidth characteristic of the mechanical design combined with the IRC and feedforward technique, accurate high-speed scans up to 400 Hz were achieved. Future research will concentrate on refining the mechanical design of the stage and its associated controller design to achieve faster scan rates and reduced coupling between various axes. The ultimate goal is to reach scan rates suitable for video-rate scanning probe microscopy with the requisite precisions.

## ACKNOWLEDGMENT

The authors would like to thank Dr. A. Fleming for his useful suggestions.

## REFERENCES

[1] S. Salapaka, A. Sebastian, J. P. Cleveland, and M. V. Salapaka, "High bandwidth nano-positioner: A robust control approach," *Rev. Sci. Instrum.*, vol. 73, no. 9, pp. 3232–3241, 2002.

[2] A. Sebastian and S. M. Salapaka, "Design methodologies for robust nano-positioning," *IEEE Trans. Control Syst. Tech.*, vol. 13, no. 6, pp. 868–876, Nov. 2005.

[3] J. Kwon, J. Hong, Y.-S. Kim, D.-Y. Lee, K. Lee, S.-M. Lee, and S.-I. Park, "Atomic force microscope with improved scan accuracy, scan speed, and optical vision," *Rev. Sci. Instrum.*, vol. 74, no. 10, pp. 4378–4383, 2003.

[4] D. Kim, D. Kang, J. Shim, I. Song, and D. Gweon, "Optimal design of a flexure hinge-based XYZ atomic force microscopy scanner for minimizing abbe errors," *Rev. Sci. Instrum.*, vol. 76, pp. 073706-1–073706-7, 2005.

[5] K.-B. Choi and J. J. Lee, "Passive compliant wafer stage for single-step nano-imprint lithography," *Rev. Sci. Instrum.*, vol. 76, pp. 075106-1–075106-6, 2005.

[6] S. Gonda, T. Kurosawa, and Y. Tanimura, "Mechanical performances of a symmetrical, monolithic three-dimensional fine-motion stage for nanometrology," *Meas. Sci. Technol.*, vol. 10, pp. 986–993, 1999.

[7] J. J. Gorman, N. G. Dagalakis, and B. G. Boone, "Multi-loop control of nanopositioning mechanism for ultra-precision beam steering," in *Proc. SPIE Conf. Free-Space Laser Commun. Active Laser Illumination III*, San Diego, CA, 2003, vol. 5160, pp. 170–181.

[8] B. G. Boone, R. S. Bokulic, G. B. Andrews, R. L. J. McNutt, and N. G. Dagalakis, "Optical and microwave communications system conceptual design for a realistic interstellar explorer," in *Proc. SPIE Conf. Free-Space Laser Commun. Laser Imag. II*, Seattle, WA, 2002, vol. 4821, pp. 225–236.

[9] S. Verma, W. Jong, Kim, and H. Shakir, "Multi-axis maglev nanopositioner for precision manufacturing and manipulation applications," *IEEE Trans. Ind. Appl.*, vol. 41, no. 5, pp. 1159–1167, Oct. 2005.

[10] G. Binnig and H. Rohrer, "The scanning tunneling microscope," *Sci. Am.*, vol. 253, pp. 50–56, 1986.

[11] G. Binnig and D. P. E. Smith, "Single-tube three-dimensional scanner for scanning tunneling microscopy," *Rev. Sci. Instrum.*, vol. 57, no. 8, pp. 1688–1689, 1986.

[12] T. Ando, N. Kodera, D. Maruyama, E. Takai, K. Saito, and A. Toda, "A high-speed atomic force microscope for studying biological macromolecules in action," *Jpn. J. Appl. Phys.*, vol. 41, no. 7B, pp. 4851–4856, 2002.

[13] J. H. Kindt, G. E. Fantner, J. A. Cutroni, and P. K. Hansma, "Rigid design of fast scanning probe microscopes using finite element analysis," *Ultramicroscopy*, vol. 100, pp. 259–265, 2004.

[14] A. J. Fleming and S. O. R. Moheimani, "Sensorless vibration suppression and scan compensation for piezoelectric tube nanopositioners," *IEEE Trans. Control Syst. Tech.*, vol. 14, no. 1, pp. 33–44, Jan. 2006.

[15] G. Schitter, K. J. Åstrom, B. DeMartini, P. J. Thurner, K. L. Turner, and P. K. Hansma, "Design and modeling of a high-speed AFM-scanner," *IEEE Trans. Control Syst. Tech.*, vol. 15, no. 5, pp. 906–915, Sep. 2007.

[16] *MicroPositioning, NanoPositioning, NanoAutomation. Solutions for Cutting-Edge Technologies*. Physik Instrumente Catalog, 2001.

[17] A. J. Fleming and S. O. R. Moheimani, "A ground-loaded charge amplifier for reducing hysteresis in piezoelectric tube scanners," *Rev. Sci. Instrum.*, vol. 76, no. 7, pp. 073707-1–073707-5, 2005.

[18] Q. Zhou and S. Devasia, "Preview-based optimal inversion for output tracking: Application to scanning tunneling microscopy," *IEEE Trans. Control Syst. Tech.*, vol. 12, no. 3, pp. 375–386, May 2004.

[19] S. S. Aphale, S. Devasia, and S. O. R. Moheimani, "High-bandwidth control of a piezoelectric nanopositioning stage in the presence of plant uncertainties," *Nanotechnology*, vol. 19, pp. 125503-1–125503-9, 2008.

[20] A. J. Fleming and S. O. R. Moheimani, "Adaptive piezoelectric shunt damping," *Smart Mater. Struct.*, vol. 12, pp. 18–28, 2003.

[21] D. Niederberger, A. J. Fleming, S. O. R. Moheimani, and M. Morari, "Adaptive multimode resonant piezoelectric shunt damping," *Smart Mater. Struct.*, vol. 18, no. 2, pp. 291–315, 2004.

[22] B. Kang and J. K. Mills, "Vibration control of a planar parallel manipulator using piezoelectric actuators," *J. Intell. Robot. Syst.*, vol. 42, no. 1, pp. 51–70, 2005.

[23] G. Schitter, P. Menold, H. Knapp, F. Allgöwer, and A. Stemmer, "High performance feedback for fast scanning atomic force microscopes," *Rev. Sci. Instrum.*, vol. 72, no. 8, pp. 3320–3327, 2001.

[24] N. Kodera, H. Yamashita, and T. Ando, "Active damping of the scanner for high-speed atomic force microscopy," *Rev. Sci. Instrum.*, vol. 76, no. 5, pp. 1–5, 2005.

[25] H. R. Pota, S. O. R. Moheimani, and M. Smith, "Resonant controllers for smart structures," *Smart Mater. Struct.*, vol. 11, no. 1, pp. 1–8, 2002.

[26] J. L. Fanson and T. K. Caughey, "Positive position feedback control for large space structures," *Am. Inst. Aeronaut. Astronaut. J.*, vol. 28, no. 4, pp. 717–724, 1990.

- [27] G. C. Goodwin, S. F. Graebe, and M. E. Salgado, *Control System Design*. Englewood Cliffs, NJ: Prentice-Hall, 2001.
- [28] S. O. R. Moheimani, B. J. G. Vautier, and B. Bhikkaji, "Experimental implementation of extended multivariable PPF control on an active structure," *IEEE Trans. Control Syst. Tech.*, vol. 14, no. 3, pp. 443–455, May 2006.
- [29] B. Bhikkaji, M. Ratnam, and S. O. R. Moheimani, "PVPF control of piezoelectric tube scanners," *Sens. Actuators A*, vol. 135, pp. 700–712, 2007.
- [30] S. S. Aphale, B. Bhikkaji, and S. O. R. Moheimani, "Minimizing scanning errors in piezoelectric stack-actuated nanopositioning platforms," *IEEE Trans. Nanotechnol.*, vol. 7, no. 1, pp. 79–90, Jan. 2008.
- [31] S. S. Aphale, A. J. Fleming, and S. O. R. Moheimani, "Integral resonant control of collocated smart structures," *Smart Mater. Struct.*, vol. 16, pp. 439–446, 2007.
- [32] Y. K. Yong and T.-F. Lu, "The effect of the accuracies of flexure hinge equations on the output compliances of planar micro-motion stages," *Mech. Mach. Theory*, vol. 43, pp. 347–363, 2008.
- [33] L. Howell, *Compliant Mechanisms*. New York: Wiley, 2001.
- [34] W. Xu and T. King, "Flexure hinges for piezoactuator displacement amplifiers: Flexibility, accuracy, and stress considerations," *Precision Eng.*, vol. 19, pp. 4–10, 1996.
- [35] N. Lobontiu, J. S. N. Paine, E. Garcia, and M. Goldfarb, "Corner-filletted flexure hinges," *Trans. ASME, J. Mech. Des.*, vol. 123, pp. 346–352, 2001.
- [36] Y. K. Yong, T.-F. Lu, and D. C. Handley, "Review of circular flexure hinge design equations and derivation of empirical formulations," *Precision Eng.*, vol. 32, no. 2, pp. 63–70, 2008.
- [37] M. Jouaneh and R. Yang, "Modeling of flexure-hinge type lever mechanisms," *Precision Eng.*, vol. 27, pp. 407–418, 2003.
- [38] F. Scire and E. Teague, "Piezodriven 50- $\mu$ m range stage with subnanometer resolution," *Rev. Sci. Instrum.*, vol. 49, no. 12, pp. 1735–1740, 1978.
- [39] K. H. Ho, S. T. Newman, S. Rahimifard, and R. D. Allen, "State of the art in wire electrical discharge machining (WEDM)," *Int. J. Mach. Tools Manuf.*, vol. 44, no. 12–13, pp. 1247–1259, 2004.
- [40] J. W. Ryu and D.-G. Gweon, "Error analysis of a flexure hinge mechanism induced by machining imperfection," *Precision Eng.*, vol. 21, pp. 83–89, 1997.
- [41] T. McKelvey, H. Akcay, and L. Ljung, "Subspace based multivariable system identification from frequency response data," *IEEE Trans. Autom. Control*, vol. 41, no. 7, pp. 960–979, Jul. 1996.



**Yuen Kuan Yong** received the B.Eng. degree (with first-class honors) in mechatronic engineering and the Ph.D. degree in mechanical engineering from the University of Adelaide, Adelaide, S.A., Australia, in 2001 and 2007, respectively.

She is currently a Research Academic at the Australian Research Council (ARC) Center for Complex Dynamic Systems and Control (CDSC), University of Newcastle, Callaghan, N.S.W., Australia. Her current research interests include the design and control of nanopositioning systems, finite-element analysis (FEA) of smart materials and structures, atomic force microscopy, and robotics.



**Sumeet S. Aphale** received the Ph.D. degree in electrical engineering from the University of Wyoming, Laramie, in 2005.

He was a Graduate Research Assistant with the Hexapod Research Laboratory, University of Wyoming. From October 2005 to June 2008, he was a Research Academic at the Australian Research Council (ARC) Center of Excellence for Complex Dynamic Systems and Control (CDSC), University of Newcastle, Callaghan, N.S.W., Australia, where he is a member of the Laboratory for Dynamics and Control of NanoSystems. In June 2008, he joined the Center for Applied Dynamics Research (CADR), University of Aberdeen, Aberdeen, U.K., as a Research Fellow. His current research interests include nanopositioning systems, vibration control, smart structures, and robotics.



**S. O. Reza Moheimani** (S'93–M'97–SM'00) received the Ph.D. degree in electrical engineering from the University of New South Wales at the Australian Defence Force Academy, Canberra, N.S.W., Australia, in 1996.

He is currently a Professor in the School of Electrical Engineering and Computer Science, University of Newcastle, Callaghan, N.S.W., Australia, where he is the Assistant Dean (Research) for the Faculty of Engineering and Built Environment. He is also an Associate Director of the Australian Research Council (ARC) Centre for Complex Dynamic Systems and Control, an Australian Government Centre of Excellence. He has held several visiting appointments at IBM Zurich Research Laboratory, Switzerland. His current research interests include applications of control and estimation in nanoscale positioning systems for scanning probe microscopy, control of electrostatic microactuators in microelectromechanical systems (MEMS), and data storage systems.

Prof. Moheimani is a Fellow of the Institute of Physics, U.K. He was the recipient of the 2007 IEEE TRANSACTIONS ON CONTROL SYSTEMS TECHNOLOGY Outstanding Paper Award. He was on the Editorial Boards of a number of journals including the IEEE. He has also been the Chairman of several international conferences and workshops.